*D. Marathe[1,2], D. Rokade[3], L. Busher Azad[3], K. Jadhav[4], S. Mahajan[4], Z. Ahmad[4], S. Gupta[4], S. Kulkarni[4], V. Juvekar[1], A. Lele[3]**

[1] *Indian Institute of Technology Bombay, India*
[2] *Maharashtra Institute of Technology, Pune, India*
[3] *CSIR-National Chemical Laboratory, Pune, India*
[4] *Reliance Industries Limited, Mumbai, India*

Effect of Plug Temperature on the Strain and Thickness Distribution of Components Made by Plug Assist Thermoforming

Plug temperature is a key parameter affecting the thickness distribution of thermoplastic components made by plug assist thermoforming. For a specified pair of plug and plastic sheet, the variation in plug temperature can alter the coefficient of friction (COF) between the pair. We show here how the temperature dependence of COF influences the nature and extent of biaxial stretching of the sheet and consequently the thickness distribution of the thermoformed component. In the present study, high impact polystyrene (HIPS) sheets were thermoformed into axisymmetric cups using a plug-assist process in which the aluminum plug temperature (T_{plug}) was varied from ambient to above the glass transition temperature of HIPS ($\sim 100\,^{\circ}C$). Biaxial strain maps on the surfaces of the formed cups were measured and quantified using Grid Strain Analysis (GSA). Thickness distributions of the cups were also measured. Temperature dependent COF between HIPS and aluminum was determined independently using a rotational rheometer. The measured COF was low for $T < 100\,^{\circ}C$, whereas it increased appreciably at and above $100\,^{\circ}C$. We conclude that when $T_{plug} < 100\,^{\circ}C$ the HIPS sheet slips on the plug during forming, and this results in biaxial stretching of the base and walls of the formed cup. In contrast for $T_{plug} > 100\,^{\circ}C$, a significant reduction in the magnitude of slip is expected. Here the sheet is gripped at the clamp and by the plug during forming which causes reduced biaxial stretching of the base and increased uniaxial stretching of the walls of the cup. Simulations of plug-assist thermoforming using a temperature dependent COF showed qualitative agreement with the GSA data thereby supporting our inferences.

1 Introduction

Thermoforming is a popular industrial process in which thermoplastic films and sheets are converted into diverse products ranging from simple beverage cups and packaging trays to complex aircraft and automotive components (Throne, 1996). In the thermoforming process, a heated thermoplastic sheet is formed into the required shape by draping over a mold using vacuum or pressure. However, uneven wall thickness distribution caused by variable localized deformation during vacuum or pressure forming often results in components having thick walls and thin base (Throne, 1991). For deep drawn components, it becomes increasingly difficult to form usable products by application of vacuum or air pressure alone. Some amount of pre-stretching of the sheet prior to forming by the use of a plug helps in even distribution of the material during forming thereby reducing thickness variations. The even redistribution of material also helps in reducing initial sheet thickness without compromising product quality (Tessier, 2014).

Plug Assist Forming (PAF) is used widely in the industry to manufacture complex deep drawn parts due to low tooling cost as compared to injection molding. A typical PAF process involves the following key steps: (a) heating of sheet above softening point, (b) pre-stretching with the help of plug, (c) application of vacuum or positive pressure and (d) cooling and trimming. Numerous parameters such as plug material, plug shape, plug temperature, plug velocity and coefficient of friction (COF) between the pair of plug and sheet affect the crucial step (b) of the PAF process. Thickness distribution in the product is a complex interplay of all such parameters.

The plug material plays a major role in PAF. Plugs made from varied classes of materials including wood, plastics, metals etc. are used in PAF (Throne, 1996). Those made out of insulating materials such as plastics and wood are 'passive' in the sense that the plug temperature depends on the contact time between the sheet and plug. On the other hand, plugs made from metals like aluminum are 'active' since their temperature can be independently controlled (Throne, 1991; 1996) and used to modulate thickness variations in the component. In recent

* Mail address: Ashish Lele, Polymer Science and Engineering Division, CSIR-National Chemical Laboratory, Dr Homi Bhabha Road, Pune 411 008, India
E-mail: ak.lele@ncl.res.in

years, syntactic foams (SF) are being used as plug material to a very large extent. Syntactic foams comprise glass, ceramic or polymeric hollow spheres embedded in a matrix or a binder, which can be epoxy, urethane or thermoplastic. The low thermal conductivity of SF foams allows for forming of sheet at lower temperature thereby reducing cycle times (Boivin and Tessier, 2011).

Besides the plug material, the sheet and plug temperatures significantly influence the thickness distribution of formed components. Aroujalian et al. (1997a; 1997b) carried out plug assist vacuum forming of HIPS sheets at different plug speeds, plug temperature and sheet temperature. They reported that at sheet temperature above softening temperature, material distribution was significantly affected by plug temperature and plug speed. Poller and Michaeli (1992) observed that plug and sheet temperatures were the major influencing parameters on wall thickness distribution in plug-assist thermoforming. Ayhan and Zhang (2000) found forming temperature to be the principle parameter influencing wall thickness distribution. Martin et al. (2009) studied plug assist forming of high impact polystyrene (HIPS) and amorphous polyethyleneterepthalate (aPET) sheets using a syntactic foam (SF) plug. It was observed for the case of HIPS that reduction in plug temperature below the glass transition temperature ($T_g \sim 100\,^{\circ}C$) led to large reduction in the thickness of the component base and corresponding increase in the thickness of the component sidewall. The use of higher plug temperatures increased the base thickness for both the materials.

For a given plug, the COF between the plug and the sheet has a major influence on the thickness distribution (Boivin, 2012). The COF is in turn dependent on the temperature of the materials sliding past each other. McCool and Martin (2010) studied plug assist forming using syntactic foam as plug material and HIPS as sheet material. They observed large reductions in the sheet thickness of the base and lower sidewall regions resulting in increased thickness of the upper sidewall at plug temperatures below 100 °C. This behavior was attributed to lower contact friction at lower plug temperatures permitting the sheet in the base to readily slide and reduce in thickness. There are several reports on the measurement of temperature dependent COF. Hegemann and Eyerer (2003) used a torsional rheometer to determine static and dynamic COF between HIPS/steel, HIPS/SF, HDPE/steel and HDPE/SF. Pairs of plug and sheet discs were glued to the parallel plates of the rheometer and the force of friction was measured at different relative velocities between the plates and at various temperatures. For HDPE/steel pair, the static COF was always higher than the dynamic COF at all temperatures except near the melt temperature where the two were identical. For HIPS/SF pair, the static and dynamic friction coefficient increased simultaneous until the glass transition temperature, whereas after T_g the static coefficient increased much more than the dynamic. Collins et al. (2001) measured both the static and dynamic coefficients of friction acting between polypropylene (PP) sheet and plugs made from Delrin, SF and aluminum at elevated temperatures. COF was measured as per ASTM-D 1894-1895. A sled made of plug materials mentioned above was pulled across the PP sheet, which was fixed in a clamp frame. The temperature of the plug materials was varied from 30 to 150 °C. Results showed that values of COF increased from 0.13 to 0.72 with increase in temperature. Martin et al. (2012) studied elevated temperature polymer-to-polymer contact friction by the sled friction test and by rotational rheometry. Sleds made of SF and polyoxymethylene were pulled across clamped HIPS and PP sheets. The sled and the clamping frame were placed in two separate temperature controlled chambers and connected through a tow-line and pulley to the universal tensile testing machine. In the rotational rheometry test the lower fixed plate of the rheometer was replaced with a plate made from the sheet material and the upper moving plate was made from the plug material. It was observed that on approaching the glass transition temperature of PS and the crystalline melting point of PP, the friction coefficients rose sharply. Morales et al. (2014) used a modified pendulous impact tester in Izod geometry to determine COF. They reported that for a fixed plug temperature, COF varied significantly with sheet temperature but not plug material. A few researchers have tried to correlate the rise in frictional force at glass transition temperature to mechanical dissipation occurring due to various relaxation mechanisms (Bueche and Flom, 1958).

Temperature and velocity dependence of COF has been studied for symmetric (polymer-on-polymer) and asymmetric (mica-on-polymer) systems using the surface force apparatus (SFA). The polymers used in the study were polystyrene (PS) and polyvinyl benzyl chloride (PVBC) (Yoshizawa et al., 1993; Hueberger et al., 1999; Luengo et al., 2000). In all cases the friction force was related to adhesion hysteresis, which was highest at temperature close to the bulk T_g. The adhesion hysteresis also depended on the load, contact time, and detachment rate (Maeda et al., 2002; Chen et al., 2005). Friction force microscopy (FFM) has also been used to study surface friction for various substrates (Bennetwitz, 2005; Michel, 1998). Temperature-controlled FFM has been used to determine the frictional character of thin polymer films (Haugstad and Gladfelter, 1996). The temperature dependence of surface friction was observed to correlate with T_g and secondary relaxation mechanisms in films of poly methyl methacrylate (PMMA), PET and PS. PMMA films showed a peak in surface frictional force around 50 °C, which is the β relaxation temperature, and also a peak at 125 °C, which is the T_g for PMMA. The dominant contribution to friction on polymer films was attributed to viscoelastic mechanical loss (Hammerschmidt et al., 1999, Sills et al., 2005). Thus it can be said that the effects of rise in frictional forces at T_g and relaxation processes observed at the macroscopic scale can be correlated to relaxation phenomenon at the mesoscopic scale.

While analytical models for understanding plug assist thermoforming have been proposed (Throne 1989; 1991), finite element methods have been predominantly used for thermoforming process simulation (Nied et al., 1990; Marchal et al., 1998; Laapin, 1999, DiRaddo et al., 2002; Weische, 2004; Martin and Duncan, 2007). The deformation response of the polymer sheet during forming has been modeled using various constitutive models such as hyperelastic models (Warby and Whitemann, 1988; Laroche et al., 2000; Warby et al., 2003, Dong et al., 2006), viscoelastic or elastic-plastic models (Bourgin et al., 1995; Nam et al., 2000; Christopherson et al., 2001; Erchiqui, 2005; Karamnou et al., 2006; O' Connora et al., 2013), and van der Waals strain energy function model (McCool and Martin, 2011). Commercially available simula-

tion software for thermoforming include T-SIM (Accuform), Polyflow (Ansys), Pam-Form (ESI) and FormView (Rheoware) (Mieghem et al., 2013). Accuracy of simulations has increased to a large extent by acquiring accurate process parameter data such as sheet temperature, plug temperature, plug displacement, stress/strain response of the polymer sheet, cavity air temperature and cavity air pressure, and by measurements of material properties such as thermal contact conductance and COF (Collins et al., 2000; Hegemann and Eyerer, 2002; Jalham, 2005; Choo et al., 2008; Morales and Candall, 2009).

Many simulations studies have highlighted the importance of plug friction during PAF (McCool et al., 2006; Martin et al., 2009). Laroche et al. (2001) evaluated a non-isothermal friction coefficient model for predicting the amount of slip in plug-assisted thermoforming which was later integrated in finite element software. Kittikanjanaruk and Patcharaphun (2013) studied the effect of sheet and mold temperature on thickness distribution. The results obtained from simulation using T-SIM were in close agreement with experimental data. T-SIM has also been used to determine the COF between sheet and plug materials (Tulsian et al., 2004; Harter et al., 2009) by fitting the simulation results to experimental data obtained by varying plug speed, temperature, depth of draw and plug shape.

From the aforementioned literature on experimental and simulation studies of PAF it is evident that plug temperature affects the thickness distribution of components, and that this effect can be related to the temperature dependence of the COF between the plug and the polymer sheet. However, a detailed study of the effect of plug temperature on the biaxial stretching of the sheet during PAF and the consequent thickness distribution has not been reported. Furthermore, there are no prior studies on simulations of the effect of plug temperature on the evolution of biaxial strain during PAF. The objective of the present study is to investigate the effect of plug temperature on the biaxial strain distribution and thickness distribution in components formed by PAF over a wide range of temperatures spanning below and above T_g. We also report here 'plug-only' experiments in which forming was done with the plug but without the application of vacuum so as to establish the effect of the plug-forming stage on thickness distribution. In our experiments, the biaxial deformation during PAF was measured and quantified in terms of aspect ratio using the Grid Strain Analysis (GSA) technique. Finite element simulations using a temperature dependent COF between the sheet and the plug were also performed for a few cases. The work presented here is organized as follows. Experimental work on PAF is described in section 2, rheology and model fitting are presented in section 3 and the main results of the work are discussed in section 4. Section 5 summarizes the conclusions of this work.

2 Materials and Methods

Three-millimeter thick HIPS sheets (grade SH731, Supreme Petrochemicals, Nagothane, India) were obtained from M/s Arihant Goldplast, Mumbai, India. Plug assist vacuum forming experiments were performed on a single stage thermoforming machine (Wonderpack SPM-55, Wonderpack, Nashik, India). The dimensions and shape of the axisymmetric aluminum mold and plug used in the experiments are shown in Fig. 1. Also shown in this figure is an 'arc', which is a curve along the surface starting from the top of the component where it is clamped to the centre of its base at the bottom.

Cartridge heaters were used to heat the plug, and its surface temperature was controlled using a resistance temperature detector coupled with a PID 313 temperature controller. The plug temperature was varied from 50 to 120 °C in steps of 10 °C. Forming was done at sheet temperature of 160 °C, which was also measured independently by a hand-held infrared thermometer. Dynamic Mechanical Analysis (DMA) experiments were performed to ascertain that the forming temperature was in the rubbery region of HIPS where thermoforming is usually carried out. Sheets were heated on either side using infrared heaters. The top surface temperature of the sheet was monitored continuously during the heating cycle using an IR temperature sensor. As soon as the top surface temperature reached 160 °C, the heaters were retracted. The bottom surface temperature was measured after the heaters retracted and was found to be 163 to 164 °C. The bottom surface temperature was slightly higher than the top surface temperature because as the sheet sags it gets closer to the bottom heater bank. The heating time for the sheet was about 120 seconds. Other parameters of the PAF process such as plug depth (80 mm), plug speed (200 mm/s) and vacuum (40 kPa) were kept constant.

Prior to forming, a grid pattern of 5 mm diameter circles was screen-printed on the HIPS sheets. Two orthogonal diameters along the length and breadth of the sheet were also printed on every circle. The spatial distribution of thickness of the formed cups was quantified by measuring the thickness at the center of

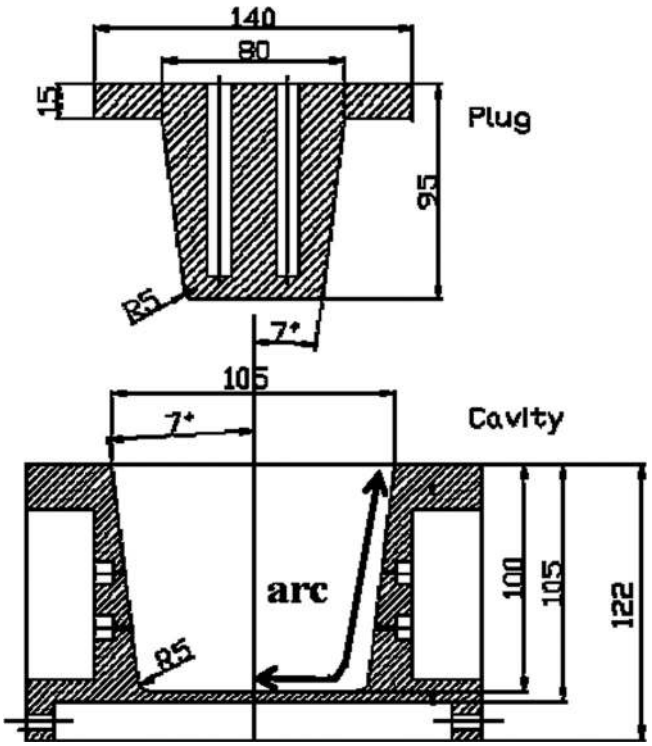

Fig. 1. Axis symmetric plug and cavity (all dimensions in mm)

each grid circle using a hand held ultra-sonic thickness gauge with a maximum error of ±2 microns over a measurement range of 30 microns to 3 mm. Thickness was measured along three arcs separated at 120° from each other. These measurements were done on 2 components and their average values and standard deviations have been reported. The grid circles deformed into elliptical shapes or larger circles depending on the nature and magnitude of strain during forming (Fig. 2). Consequently, the two diameters of the grid circles also deformed into two axes of the corresponding ellipses. The lengths of these axes were used to quantify the local surface strains of the thermoformed component using the technique of Grid Strain Analysis (GSA) (Sowerby et al., 1982; Schaeffler, 2006). Surface strains are defined as the absolute difference between the diameter of the original circles and the lengths of the axes of the corresponding ellipses formed after deformation, normalized by the diameter of the original circles (5 mm). Thus local surface strains can be defined along the two directions of the axes of the ellipse. The results described in this work are based on the choice of two specific directions: Direction-1 is along an arc that is so chosen that one of the axes (axis-1) of the deformed ellipses that lie along the arc coincides with the arc, and Direction-2 coincides with the other axis (axis-2) of the deformed ellipse (see Fig. 2).

Dimensions of the two axes of each ellipse were measured using a Co-ordinate Measuring Machine (CMM) (Cordimeasure E01-01, Accurate). An electronic touch trigger probe (Reinshaw, Wotton-under-Edge, UK) comprising a 1 mm diameter spring loaded steel ball stylus controlled by a hand box with a joystick was used for the measurements. For any given ellipse, the dimensions of its axes (oriented along axis-1 and axis-2) were measured by positioning the probe on several points along the axes and adding the (small) linear distance between these points. The surface strains along the two axes were calculated from the measured dimensions. Besides the surface strains, we have also used the aspect ratio of the ellipses as a measure of the local deformation. The aspect ratio is defined here as the ratio of the lengths of axis-2 and axis-1 of the ellipses along the arc.

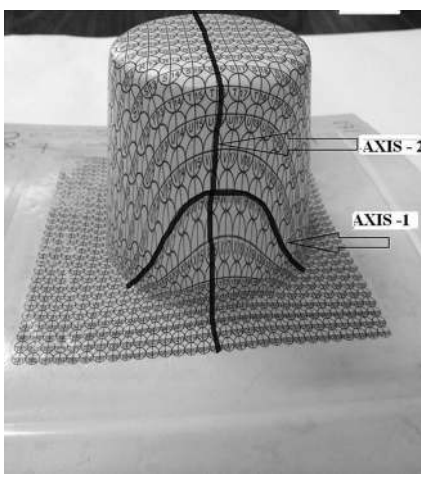

Fig. 2. Formed component showing deformed grid circles at plug temperature 120°C

In addition to the PAF experiments described above, 'plug-only' experiments were carried out for each plug temperature to assess the effect of the plug assist step on the thickness distribution. Forming was stopped prior to vacuum application and the component was cooled for one minute till the temperature reached around 70 °C. Thickness measurements were carried out along 3 arcs separated at 120° for each component. Average values and standard deviation for 2 such components have been reported.

Temperature dependent COF was determined using a strain-controlled rotaional rheometer (ARES-G2, TA Instruments, New Castle, USA). Steady shear tests at a shear rate of 7.85 s^{-1} under a normal force of 4N were conducted using a 25 mm aluminum disposable parallel plate geometry with HIPS discs glued to the lower plate. The disposable alumimum plates had a R_a value for surface roughness of 0.8 microns while that for the plug was 1.1 microns which are very close.The lower plate was rotated at 0.628 rad/s. The normal force of 4 N was applied to ensure proper contact between the top plate and the HIPS disc. Measurements were made between 50 to 120 °C in steps of 10 °C. The COF was calculated using the following Eq. 1:

$$\mathrm{COF} = \frac{1.5}{R}\left(\frac{T}{F}\right), \tag{1}$$

where T is the torque, F the normal force and R is the sample radius. The numerical factor 1.5 in Eq. 1 is used as a correction for the velocity gradient over the circular sample surface (Hegemann and Eyerer, 2003; Lee et al., 2001). The data of measured torque v/s time for different temperatures is shown in Fig. 3. The oscillations in torque vs. time are observed due to dynamic slip-stick nature of contact between the upper parallel plate and HIPS discs. The details of the torque patterns are not relevant to our analysis, however average values of torque calculated from many oscillations have been used to calculate an average value of COF. Dependence of COF on normal force was assessed by carrying out the experiments at 4 N, 7 N and 10 N force and the COF was calculated from Eq. 1. No significant variation in COF was observed. Hence a normal force of 4 N was used for all experiments. Table 1 shows the results of the COF experiments.

3 Rheology, Model Fitting and Simulation

Simulations of the plug assist vacuum forming process were carried out using commercial software (T-SIM, version 4.81, Accuform, Zlin, Czech Republic). Following Lee et al. (2001) who used the K-BKZ constitutive equation in T-SIM to fit the uniaxial elongational data for ABS and subsequently used it for forming simulations, we used the K-BKZ constitutive equation with Wagner I damping function (Eq. 2) to model the viscoelastic properties of HIPS.

$$\sigma(t) = -\int_{-\infty}^{t}\sum_{i=1}^{N}\frac{G_i}{\lambda_i}\exp\left(-\frac{t}{\lambda_i}\right)\left(\frac{1}{[1+\alpha\sqrt{(I_1-3)*I_2-3)}]}\right) C^{-1}(t,t')dt', \tag{2}$$

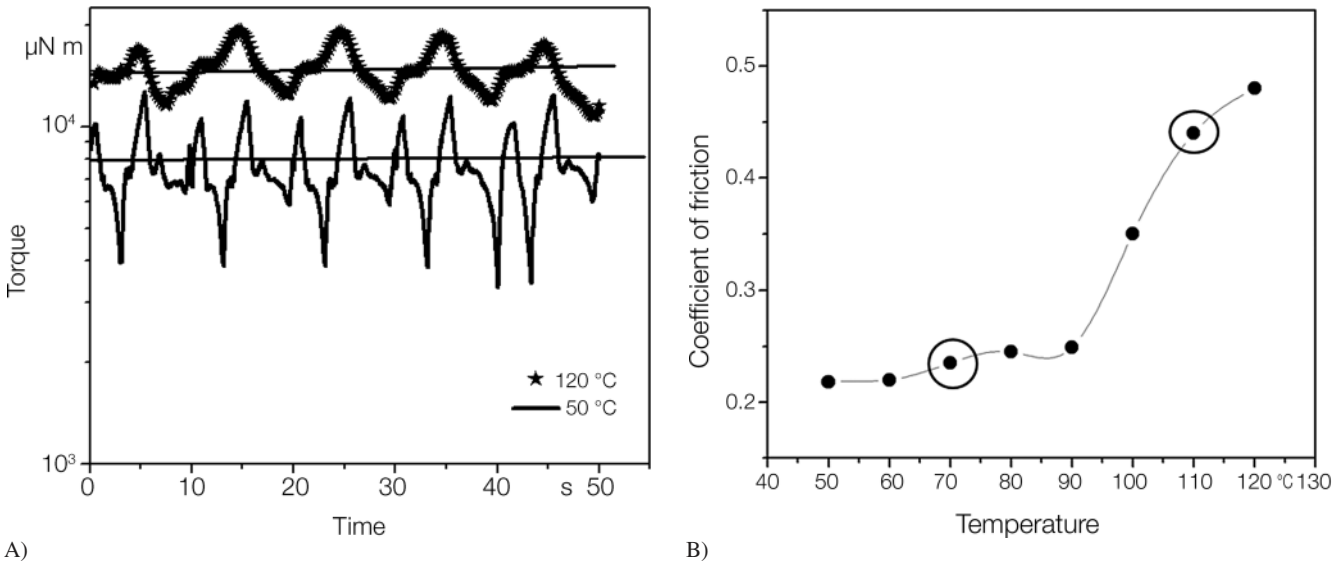

Fig. 3. Torque vs. time for representative temperatures above and below T_g, the horizontal lines indicate average torque values (A), experimentally measured temperature dependent COF for HIPS/aluminum pair, encircled points are the COF values that were used in simulations at 70 °C and 110 °C (B)

S. No.	Temperature °C	Normal force N	Average torque $\times 10^{-6}$ N m	Standard deviation of average torque	Average torque/normal force $\times 10^{-6}$ m	COF
1	50	4	7573	160.1	1893	0.227
2	60	4	7595	72.1	1898	0.228
3	70	4	7821	80.1	1955	0.234
4	70	7	13727	160.6	1961	0.235
5	70	10	18780	34.3	1878	0.225
6	80	4	8019	18.5	2022	0.24
7	90	4	8228	39.8	2057	0.246
8	100	4	11574	180.1	2893	0.347
9	110	4	14825	105.5	3706	0.444
10	120	4	16026	110.1	4006	0.481

Table 1. COF results

$\sum_{i=1}^{N} \frac{Gi}{\lambda_i} \exp\left(-\frac{t}{\lambda_i}\right)$ in Eq. 2 is the memory function and G_i and λ_i are respectively the relaxation moduli and relaxation time of mode i. $\sigma(t)$ is the stress tensor, C^{-1} is the inverse Cauchy-Green tensor, I_1 and I_2 are first and second invariants of the inverse Cauchy-Green strain tensor, and α is an adjustable parameter. Linear viscoelastic properties of HIPS were determined by carrying out Small Amplitude Oscillatory Shear (SAOS) tests on a strain-controlled rheometer (ARES, TA Instruments, New Castle, USA) using parallel plate geometry (25 mm diameter plates, 1 mm gap). Under conditions of the SAOS test, the value of the damping function in Eq. 2 becomes equal to one and consequently the K-BKZ model reduces to the Lodge model (or equivalently, to the Maxwell model in scalar form). Thus in SAOS flow the K-BKZ model predicts the following equations for the dynamic storage modulus G′ and loss modulus G″:

$$G' = \sum_i G_i \frac{\omega^2 {\lambda_i}^2}{1+\omega^2 {\lambda_i}^2} \quad G'' = \sum_i G_i \frac{\omega \lambda_i}{1+\omega^2 {\lambda_i}^2}, \tag{3}$$

where ω is frequency, G_i is relaxation modulus and λ_i is relaxation time. To obtain the material parameters $\{\lambda_i, G_i\}$ SAOS tests were performed over a temperature range of 150 to 200 °C and over a frequency range of 0.01 to 100 rad/s to get the dynamic moduli, $G'(\omega)$ and $G''(\omega)$. This data was then shifted horizontally along the frequency axis using the Time-Temperature Superposition principle to a reference temperature of 150 °C (Fig. 4) to obtain master curves. Subsequently, a discrete 8-mode relaxation spectrum $\{\lambda_i, G_i\}$ and WLF shift factors $\{a_T\}$ were obtained by fitting Eq. 3 to the master curve.

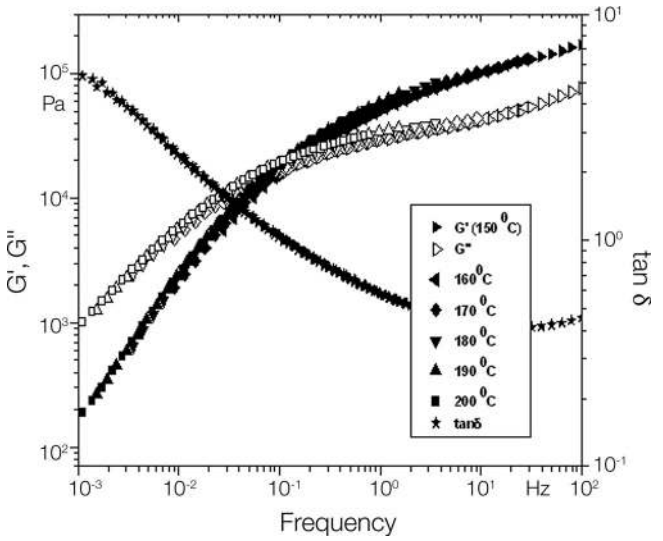

Fig. 4. Time-temperature superposition obtained from SOAS

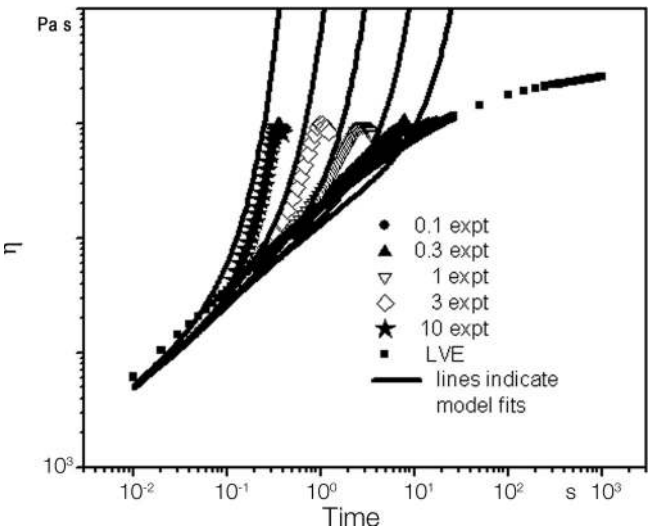

Fig. 5. KBKZ Wagner I fits for extensional data

For extensional flows, where deformation is non-linear, the inverse of Cauchy Green strain tensor reduces to

$$\begin{bmatrix} 1/\lambda_1^2 & 0 & 0 \\ 0 & \lambda_1 & 0 \\ 0 & 0 & \lambda_1 \end{bmatrix},$$

where λ_1 is the extension ratio in flow direction.

$$I_1 = \frac{1}{\lambda_1^2} + 2\lambda_1 \quad \text{and} \quad I_2 = \frac{2}{\lambda_1} + \lambda_1^2.$$

Hence, the equation for extensional stress is given by,

$$\sigma_{11}(t) = \int_{-\infty}^{t} \sum_{i=1}^{N} \frac{G_i}{\lambda_i} \exp\left(-\frac{t}{\lambda_i}\right) \left(\frac{1}{[1+\alpha\sqrt{(I_1-3)*(I_2-3)}]}\right)\left(\frac{1}{\lambda_1^2} - \lambda_1\right), \quad (4)$$

from which tensile stress growth function can be calculated as

$$\eta_e^+ = \frac{\sigma_{11}(t)}{\dot{\varepsilon}}. \quad (5)$$

This equation was fit to the experimental uniaxial extensional data to find the value of α in Eq. 2. Extensional experiments were carried out using the SER Universal Testing Platform from Xpansion Instruments, Tallmadge, USA, which works on the rheometer and records the tensile stress growth coefficient as a function of time at different stretch rates. Tensile stress growth was measured at stretch rates varying from 0.1 to 10 s^{-1} at 150 °C. Figure 5 shows fitting of extensional viscosity data to K-BKZ Wagner I viscoelastic model for $\alpha = 0.001$. The model fits well the onset of strain hardening; however it fails to predict the steady-state extensional viscosity due to the particular choice of the damping function. The value of α along with the relaxation spectrum $\{\lambda_i, G_i\}$ and WLF shift factors $\{a_T\}$ were used as material input parameters in the forming simulations. The T-SIM software used in this work deploys a finite element Lagrangian mesh. Mesh density optimization was carried out prior to simulations. Convergence was achieved above mesh density of 60 000 elements. Mesh density of 100 000 was used for the present simulations. It was observed that amongst all the input parameters, thickness distribution and surface strain were most sensitive to COF.

4 Results and Discussion

Figure 6A shows the regions in wall thickness distribution of the axisymmetric cup made by PAF process at representative plug temperatures above and below T_g. The x-axis denotes positions on the cup along the arc that starts at the top of the cup and ends at the center of the base as described earlier (Fig. 1). The thickness distribution can be analysed in 3 regions: base, lower sidewall and upper sidewall. During forming, the sheet is stretched between the clamping frame and plug base. The corners are usually the thinnest. The plug mark, which is seen distinctly as the maximum thickness along the sidewall, differentiates the regions of the sheet that are affected and unaffected by the plug. The plug mark appears in the region of the sidewall where the sheet loses contact with the plug and gets stretched as a free surface between the clamping frame and the plug. Prior to the plug stage, the sheet sags upon heating and comes in contact with the upper portion of the cold cavity thereby resulting in local cooling in that region. As a result it is difficult to draw material from the upper sidewalls during the plug stretching stage, which leads to a thicker upper sidewall. This is immediately followed by a thinner portion of the upper sidewall caused by the drawing action of the plug. In the final forming stage after the plugging stage, vacuum is applied in order to give requisite shape to the component. This does not alter the nature of deformation but adds to the amount of deformation.

As mentioned in section 2, plug assisted vacuum forming of HIPS cups were performed at various plug temperatures in the

range 50 to 120 °C. For sake of clarity, Fig. 6A shows the thickness distribution of cups formed only at four representative plug temperatures, two below the T_g of HIPS and two above the T_g. The differences in the thickness distributions of the components formed above and below the T_g are clearly evident in these figures. Figure 6B shows thickness data with standard deviation for only two temperatures, above and below T_g. The differences in the thickness distributions for the two forming temperatures are well beyond the standard deviation indicating that the differences are real. It can be seen from Fig. 6A and B, that at plug temperatures above the T_g of HIPS, the thickness of the base of the component is high. With decrease in plug temperature below 100 °C, considerable reduction of base thickness is observed. Also, a clear plug mark is seen for cups made at plug temperatures above the T_g. The plug mark smoothens out as the temperature decreases below the T_g.

To emphasize the predominant effect of the plug on the thickness distribution, 'plug only' experiments were carried out. It may be noted that the deformation in this case is only due to the motion of the plug. Figure 7A shows the thickness distribution for four representative temperatures two above and two below T_g, while Fig. 7B shows the same data along with standard deviation for two of the four representative temperatures. Once again, the differences in the thickness data at the two forming temperatures are evident and are well beyond the measured standard deviations.

We now present results on surface strains measured by the GSA technique. To recollect, surface strain along an axis is de-

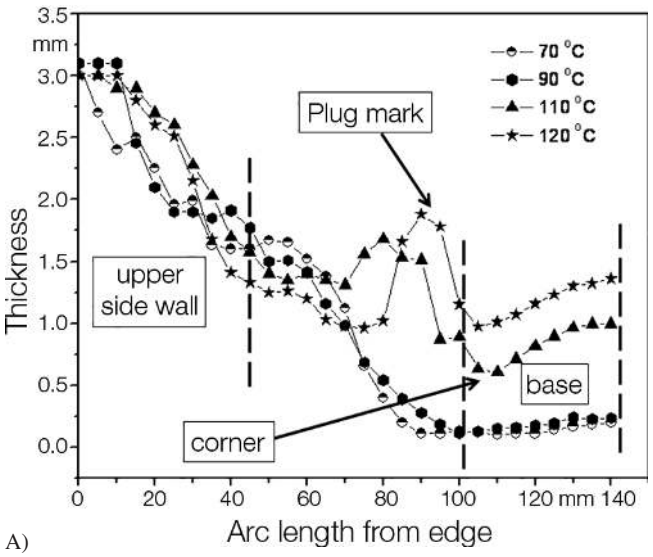

A)

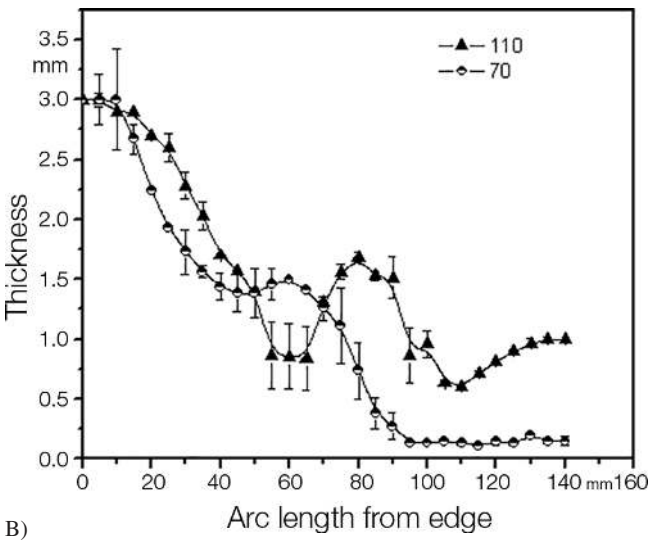

B)

Fig. 6. Thickness distribution in PAF for plug temperatures above and below T_g indicating typical features in wall thickness distribution (A), thickness distribution in PAF with standard deviation at representative temperatures above and below T_g (B)

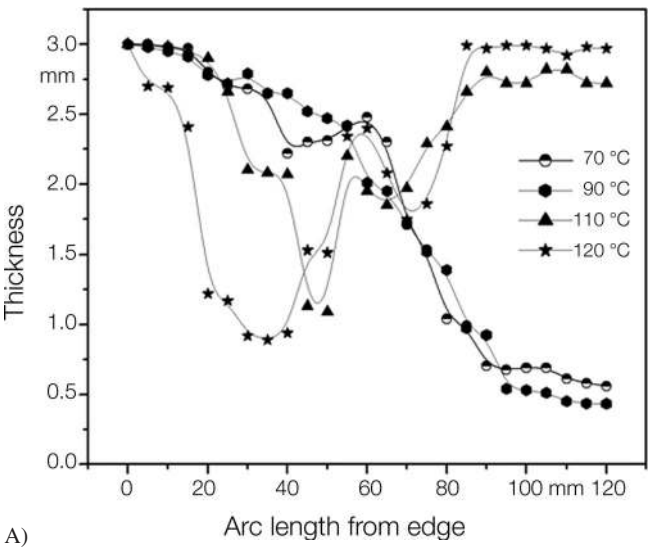

A)

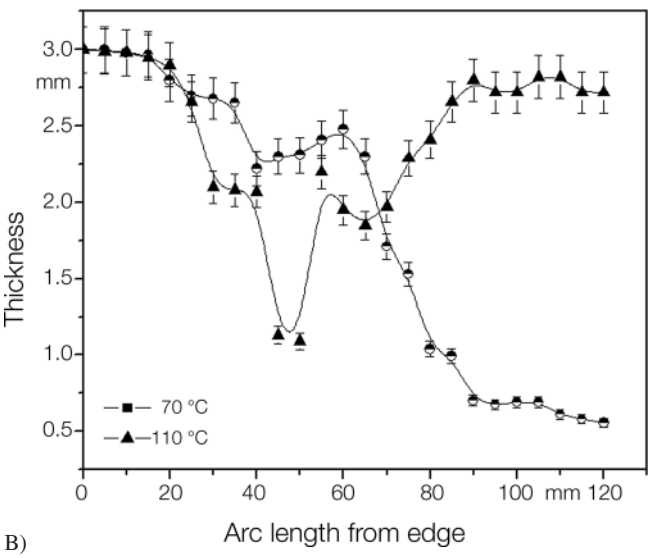

B)

Fig. 7. Thickness distribution for plug only experiments (A) and thickness distribution for plug only experiments with standard deviation at representative plug temperatures (B)

fined here as the ratio of change in dimension along that axis to the original dimension. Consequently, the surface strain can be zero in case of no deformation or positive/negative if deformation along the axis is greater/lesser than original diameter of the grid circle. Figure 8A and B show surface strains along axis-1 and axis-2, respectively for the same four representative forming temperatures. From Fig. 8A it can be seen that in the upper sidewall region, the surface strain-1 (surface strain along axis-1) is slightly negative indicating slight compression along axis-1. However everywhere else along the arc, the surface strain-1 rises monotonically for all plug temperatures. A small decrease in the strain is observed near the center of the base. It can be seen that any given arc length, the surface strain-1 decreases monotonically with temperature. The pattern of surface strain-2 (surface strain along axis-2) is non-monotonic for all plug temperatures as can be seen in Fig. 8B. The surface strain-2 increases along the upper sidewall, then decreases along the lower sidewall and finally increases again along the base region. In the side-wall region the surface strain-2 is higher for the higher temperatures ($T > T_g$) and lower for the lower temperatures ($T < T_g$). This pattern is reversed in the base region of the component. For the upper sidewall region the high surface strain-2 coupled with low surface strain-1 clearly indicates uniaxial extension along direction 2. In contrast for the base region, the strains along the axis 1 and 2 are simultaneously high indicating biaxial stretching in this region.

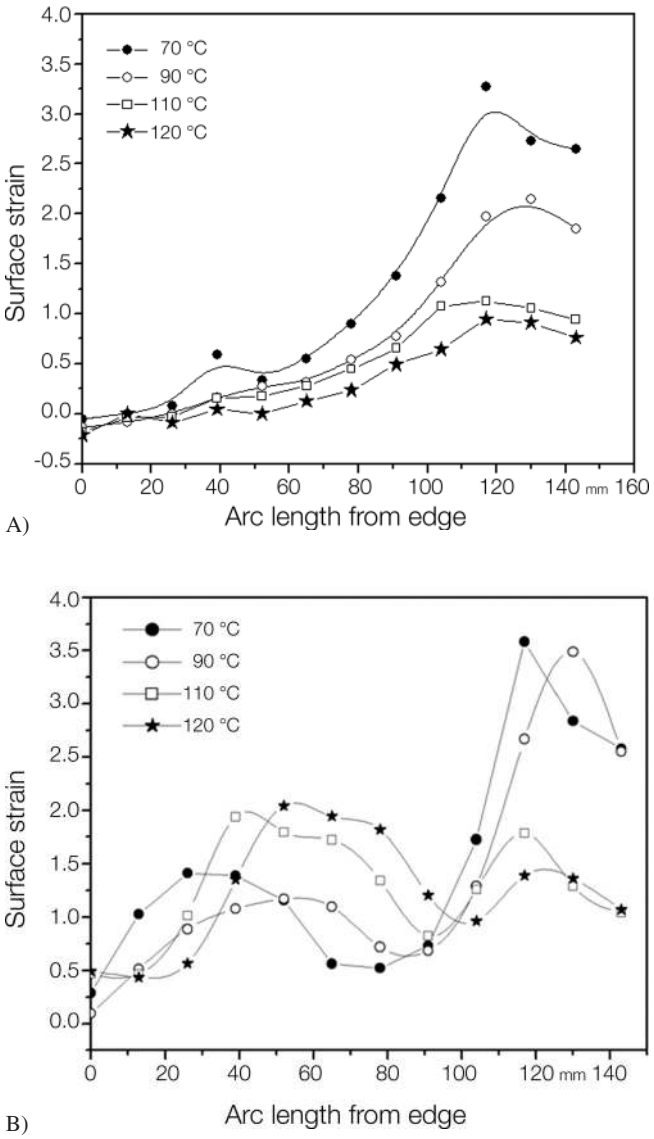

Fig. 8. Surface strain along axis-1 (A) and axis-2 (B)

In order to assess the temperature dependence of COF, experimental determination of COF was carried out using a rotational rheometer for the temperature range 50 to 120 °C in steps of 10 °C as mentioned earlier. It can be seen from Fig. 3B and Table 1 that the average COF increases gradually from 0.218 to 0.25 between 50 °C and 90 °C. As the temperature nears the T_g, the COF rises rapidly to 0.35 at 100 °C and to further 0.5 at 120 °C. The oscillations in torque also reduce in amplitude and frequency as the temperature crosses T_g. These results show similar trends as those reported by Hegemann and Eyerer (2003) and Martin et al. (2012).

The experimental data for the temperature dependence of component thickness, biaxial strains and COF can now be discussed together. First we look at the thickness distribution. A simplistic argument based only on heat transfer rates might suggest that lower plug temperatures would lead to rapid conductive heat transfer between sheet and plug leading to decrease in sheet temperature and hence thicker base of the component, while higher plug temperatures would result in a thinner base. However, the experimental data shows exactly the opposite. This is on account of the fact that cooling of the sheet also influences the friction between the plug and the sheet. The COF data shows that at temperatures below T_g the COF is lower indicating that the HIPS tends to slip along the aluminum plate. On the other hand, at temperatures above T_g the COF is higher indicating that the HIPS tends to stick to the aluminum plate. As discussed in section 1, frictional behavior is related to viscoelastic losses. At temperatures below T_g since viscoelastic losses are negligible, the sheet does not stick to the plug but in fact predominantly slips along the plug surface. This allows the material to slide from the base towards the sidewall resulting in thinner base of the component. At the same time, the plug mark is pushed towards the upper sidewall. In contrast for plug temperatures near T_g, the viscoelastic loss becomes significant and when the plug-sheet interfacial temperature reaches T_g the stick behavior becomes predominant. Consequently, the sheet sticks to the plug at the base resulting in higher base thickness. The plug mark is predominant and shifts towards the base. Thus, the results show that temperature dependent friction is the predominant factor determining the thickness distribution, and these are in agreement with the results of Martin and Duncan (2007) and McCool and Martin (2010).

For the 'plug-only' experiment at 120 °C the base thickness is around 3 mm (Fig. 7A and B), which is almost equal to the initial sheet thickness therefore indicating no-slip behavior between the plug and the sheet at this temperature. But for plug temperatures below 100 °C, the base is thinner indicating slip behavior between sheet and plug base. Thus in addition to thickness distribution results obtained in PAF experiments, the 'plug-only' results co-relate well with results of COF ex-

periments. This re-emphasizes the primary role of plug temperature on the thickness distribution.

Coming now to the biaxial strain distribution results, for temperatures above 100 °C the strains along both axes are low for the base region indicating lesser biaxial deformation. Also at these temperatures, the surface strain-1 on the sidewalls is higher than the surface strain-2 indicating predominantly uniaxial deformation along the sidewalls (Fig. 8B). Thus it is clear that at plug temperatures greater than T_g, the sheet stretches uniaxially along the side walls but does not stretch much along the base. As already mentioned, the 'stick' boundary condition is predominant between the plug and the sheet at these temperatures. Thus at the component base, where the sheet is in contact with the plug, the sheet remains anchored. It is also anchored at the clamping frame, and hence as the plug moves down the sheet stretches uniaxially along the sidewalls. As mentioned earlier, vacuum applied after the plugging stage does not alter the nature of deformation but adds to it.

For plug temperatures below T_g, the 'slip' boundary condition is predominant between the plug and the sheet. Hence during the plug motion, the sheet slips along the plug at the base of the component and is therefore drawn biaxial. This is seen from the high values of surface strains along both the axes in the base region in Fig. 8A and B. Consequently, the sheet is anchored to a lesser extent between the base and clamping frame and hence the extent of uniaxial stretching in the wall region is lower at plug temperatures $< T_g$ relative to the case of plug temperatures $> T_g$. This is seen from lower values of surface strain-1 along the sidewall as compared to surface strain-1 values for higher plug temperature. Figure 9A and B indicate photographs of component base at plug temperatures above and below T_g while Fig. 9C and D show photographs of component sidewalls at $T_{plug} > T_g$ and $T_{plug} < T_g$. It can be seen in Fig. 9A and B that the grid circles are larger at plug temperatures below T_g, indicative of larger strain at the base as compared to that above T_g. Figure 9C and D show that the grid circles are transformed into ellipses with their major axis along axis-2 being larger for $T_{plug} > T_g$ than for $T_{plug} < T_g$ indicating uniaxial extension along axis-2 for plug temperatures greater than T_g.

The before mentioned trends can also be illustrated by using the aspect ratio of the ellipses, which are shown in Fig. 10. A ratio of unity indicates equibiaxial stretch, a ratio > 1.0 indicates tendency to stretch uniaxially along axis-2 and a ratio < 1.0 indicates tendency to stretch uniaxially along axis-1. Figure 10 shows greater uniaxial extension for the sidewalls at 110 °C and 120 °C as compared to lower temperatures, whereas near equibiaxial deformation is seen at the base for all plug temperatures. Thus, the deformation along the sidewalls is predominantly uniaxial, especially for $T_{plug} > 100$ °C.

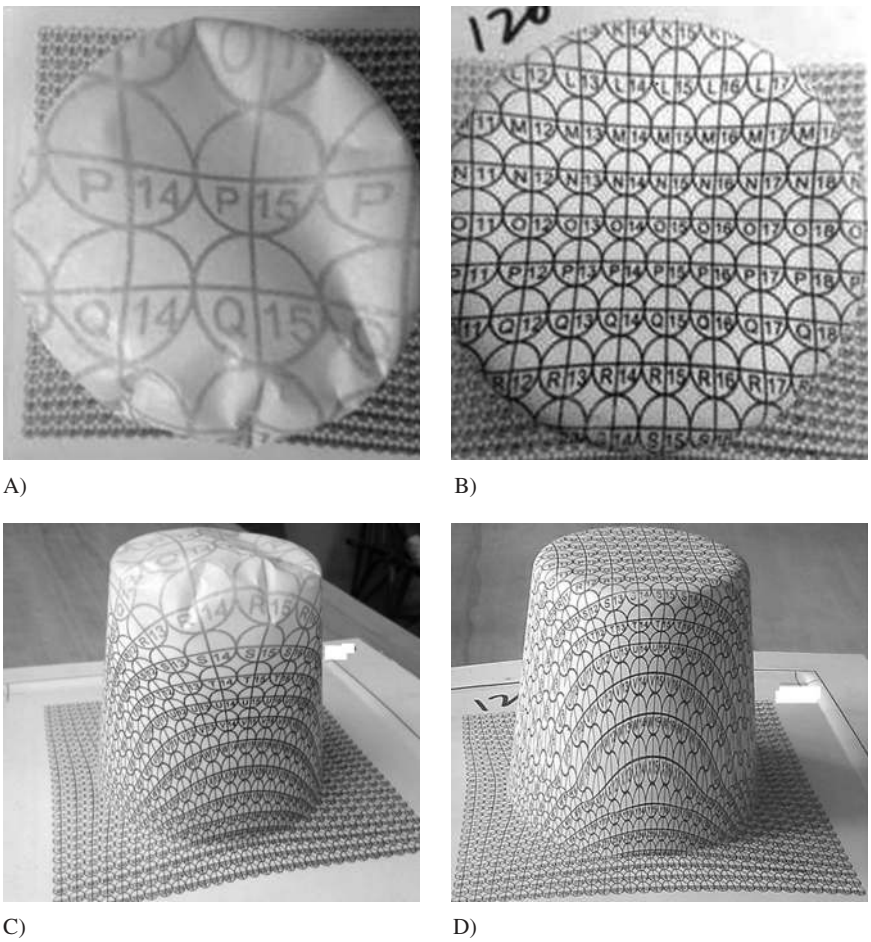

Fig. 9. Component base at 70 °C (A), 120 °C (B) and component side walls at 70 °C (C) and 120 °C (D)

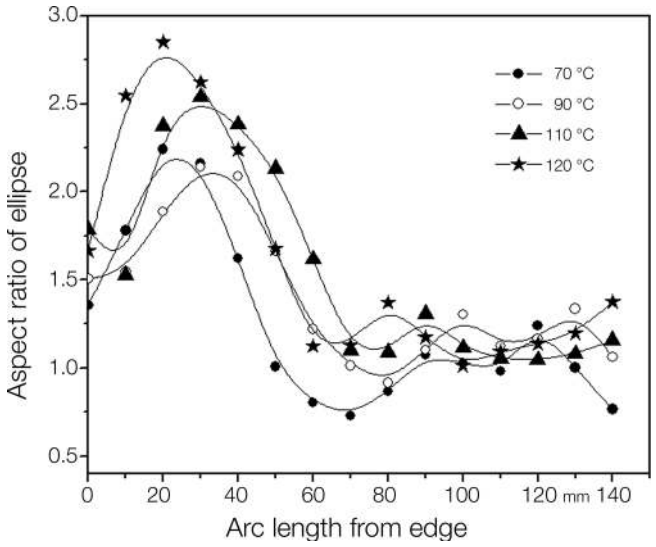

Fig. 10. Aspect ratio for the ellipses

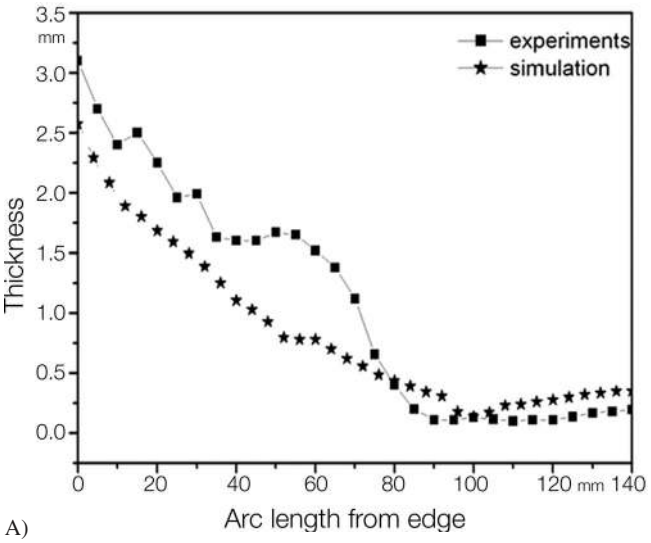

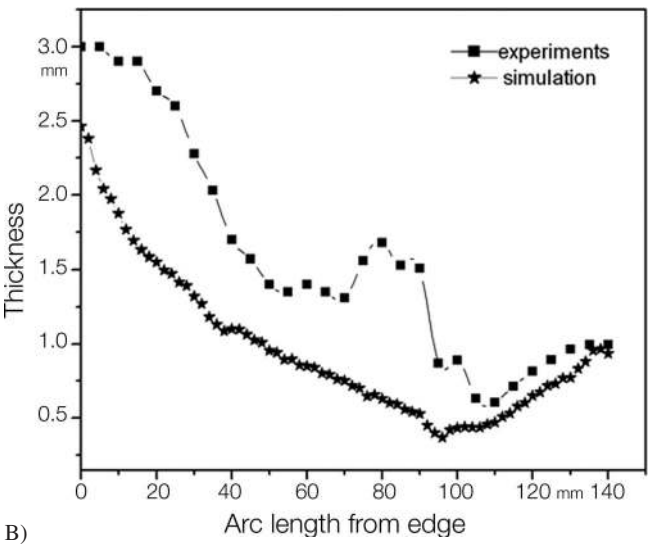

Fig. 11. Comparison of thickness distribution by experiments and simulation for 70 °C (A) and at plug temperature 110 °C (B)

We now present results of PAF simulations, which were performed using the constitutive model described in section III. The simulations were performed only to qualitatively ascertain the hypothesis that stick/slip behavior at the sheet-plug interface governs the thickness and biaxial strain distribution in the component during forming. Two representative simulations were carried out at plug temperature of 70 °C and 110 °C, which are respectively above and below T_g using the experimentally determined COF. Figure 11A and B show comparison between experimental and simulated thickness distribution of the component. The simulation results are in qualitative agreement with experimental data except for the plug mark. In particular, the simulations correctly predict the lower thickness of base at 70 °C ($T_{plug} < T_g$) and larger base thickness at 110 °C ($T_{plug} > T_g$). These results are similar to those obtained by Lee et al. (2001) and Kittikanjanaruk and Patcharaphun (2013).

Further, Fig. 12A and B show the predicted surface strains for the same two plug temperatures of 70 °C and 110 °C. Except for the region along the lower side-wall where the sheet leaves the plug, the salient features of the predicted strains are in fair agreement with the experimental results shown earlier in Fig. 8A, B. For example, the surface strain-1 increases monotonically till a point inside the base region followed by a slow decrease till the center of the base. Also, the surface strain-2 in the base region is greater for $T_{plug} = 70$ °C than for $T_{plug} = 100$ °C. Similarly the surface strain-2 shows two maximums, one along the sidewall and the other along the base. The surface strain-2 along the sidewall is greater for $T_{plug} = 100$ °C than for $T_{plug} = 70$ °C,while the trend is reversed for the base of the component. The simulations predict equibiaxial stretching along the base and uniaxial stretching along axis-2 along the sidewall, which is higher for $T_{plug} = 100$ °C than for $T_{plug} = 70$ °C. These predictions are also in qualitative agreement with the experimental data shown in Fig. 10.

The differences between the experimental results and simulations may arise due to several reasons. In experiments, some material from the clamped surface of the sheet gets drawn into the cavity during forming as can be seen in Fig. 9C and D. In the simulations, however the surface was assumed to have no slip boundary condition, which prevents any drawing of material in the cavity. This can be one reason why the experimentally determined thickness is greater than that obtained from simulations (see Fig. 11A and B). Also, it is difficult to predict the point of separation of the sheet from the plug because of the discontinuity in boundary conditions between the region where the sheet drapes the plug and the free sheet. As a result, the simulations are unable to predict the plug mark (see Fig. 11A and B). Furthermore, the KBKZ constitutive equation does not quantitatively capture all aspects of rheological behavior of the HIPS melt. As can be seen from Fig. 5, even though the experimental data might reach steady state, the predicted elongational viscosity continues to show strain hardening. Despite these obvious differences, the simulations are in qualitative

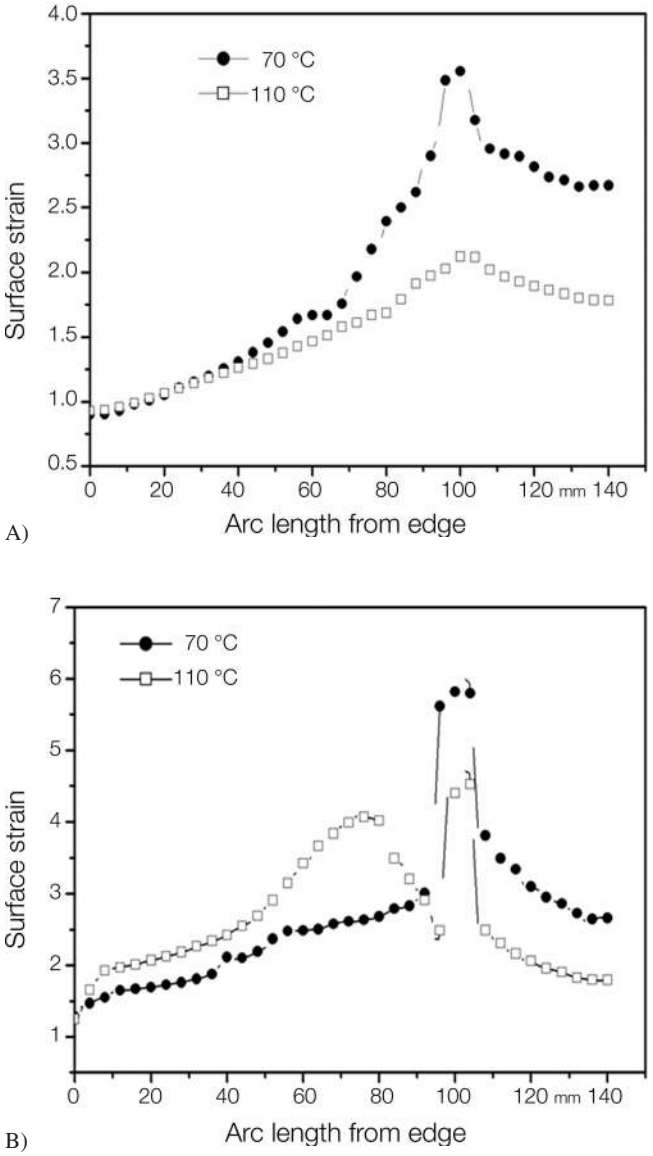

Fig. 12. Surface strains along axis 1 (A) and along axis 2 (B) from simulation

agreement with the experimental results and are useful for validation of the hypothesis that variation in plug temperature causes the variation in COF which affects surface strain distribution.

5 Conclusion

Plug assist thermoforming experiments were carried out at various plug temperatures keeping constant the plug material (aluminum) and sheet material (high impact polystyrene).

Axisymmetric cups were thermoformed and their surface strain distribution and thickness distribution were experimentally measured and quantified using Grid Strain Analysis technique. It was found that the plug temperature plays a significant role in governing the surface strain distribution and thickness distribution of the components. Independent friction measurements between HIPS and aluminum showed that the COF increased rapidly over a narrow temperature range near the Tg from 0.227 at 90 °C to 0.481 at 120 °C. This modulation of the contact friction results in a significant difference (on average ~85 %) for the base thickness when thermoformed at temperatures below and above the T_g. Similarly, the difference in surface strains for components formed above and below T_g was as much as 55 % and 69 % respectively for axis-1 and axis-2. The COF measurements suggest a greater slip between the plug and the sheet in case of plug temperatures lower than the glass transition temperature. This caused thinning of the component base and reduced uniaxial extensional deformation of the sidewall of the component. In case of forming experiments wherein the plug temperature was equal to or higher than the glass transition temperature of the sheet, reduced slip between the plug and sheet resulted in higher thickness of the base of the component and higher uniaxial extension of the sidewall. 'Plug-only' experiments validated the predominant effect of plugging stage on the final thickness distribution. Simulations were performed using a viscoelastic constitutive model for the polymer sheet and using temperature dependent coefficient of friction between the plug and the sheet. The simulated surface strain distribution and thickness distribution showed qualitative agreement with experimental results.

References

Aroujalian, A., Ngadi, M. and Emond, J., "Effect of Processing Parameters on Compression Resistance of A Plug-Assist Vacuum thermoformed Container", Adv. Polym. Tech., **16**, 129–134 (1997a), DOI:10.1002/(SICI)1098-2329(199722)16:2<129::AID-AD-V5>3.0.CO;2-W

Aroujalian, A., Ngadi, M. and Emond, J., "Wall Thickness Distribution in Plug-Assist Vacuum Formed Straw Berry Containers", Polym. Sci. Eng., **37**, 178–182 (1997b), DOI:10.1002/pen.11659

Ayhan, Z., Zhang, Q. H., "Wall Thickness Distribution in Thermoformed Food Containers Produced ba a Benco Aseptic Packaging Machine", Polym. Eng. Sci., **40**, 1–10 (2000), DOI:10.1002/pen.11134

Bennewitz, R., "Friction Force Microscopy", Mater. Today, **8**, 42–48 (2005), DOI:10.1016/S1369-7021(05)00845-X

Boivin, K., "Optimizing the Cut Sheet Thermoforming Process with Syntactic Foam", Thermoforming Quarterly, **31**, 6–12 (2012)

Boivin, K., Tessier, N, "Epoxy Syntatic Foams for Use as Plug Assist in Heavy Gauge Thermoforming", SPE ANTEC Tech. Papers, 1–4 (2011)

Bourgin, P., Cormeau, T. and Matin, C., "A First Step towards the Modelling of the Thermoforming of Plastic Sheets", J. Mater. Process. Technol., **54**, 1–11 (1995), DOI:10.1016/0924-0136(95)01910-3

Bueche, A. M., Flom, D. G., "Surface Friction and Dynamic Mechanical Properties of Polymers", Wear, **2**, 168–182 (1958), DOI:10.1016/0043-1648(59)90002-X

Chen, N., Maeda, N., Tirrel, M. and Israelchvili, J., "Adhesion and Friction of Polymer Surfaces: The Effect of Chain Ends", Macromolecules, **38**, 3491–3503 (2005), DOI:10.1021/ma047733e

Choo, H., L., Martin, P. and Harkin-Jones, E., "Measurement of Heat Transfer for Thermoforming Simulations", Int. J. Mater. Form., **1**, 1027–1030 (2008), DOI:10.1007/s12289-008-0233-7

Christopherson, R., Debbaut, B. and Rubin, Y., "Simulation of Pharmaceutical Blister Pack Thermoforming Using a Non-Isothermal Integral Model", J. Plast. Film Sheeting, **17**, 239–251 (2001)

Collins, P., Martin, P., Harkin-Jones, E. and Laroche, D., "Experimental Investigation of Slip in Plug-Assisted Thermoforming", SPE's ANTEC Conference Proceedings, 630 – 635 (2001)

Collins, P., Lappin, J., Harkin-Jones, E. and Martin, P., "Investigation of Heat Transfer in the Plug Assisted Thermoforming Process", SPE's ANTEC Conference Proceedings, 788 – 792 (2000)

D'Oria, F., Bourgin, P. and Coincenot, L., "Progress in Numerical Modeling of the Thermoforming Process", Adv. Polym. Tech., **14**, 291 – 301 (1995), DOI:10.1002/adv.1995.060140403

Diraddo, R., Girard, P. and Chang, S., "Model-Based Control of Material Distribution in Thermoformed Parts–, SPE's ANTEC Conference Proceedings ,722 – 726 (2002)

Dong, Y., Lin, R. and Bhattacharyya, D., "Finite Element Simulation on Thermoforming Acrylic Sheets Using Dynamic Explicit Method", Polym. Polym. Compos., **14**, 307 – 328 (2006)

Erchiqui, F., "Thermodynamic Approach of inflation Process of K-BKZ Polymer Sheet with Respect to Thermoforming", Polym. Eng. Sci., **45**, 1319 – 1335 (2005), DOI:10.1002/pen.20360

Hammerschmidt, J., Moasser, B. and Gladfelter, W., "Polymer Viscoelastic Properties Measured by Friction Force Microscopy", Macromolecules, **32**, 8996 – 8998 (1999), DOI:10.1021/ma981966m

Harter, C. S., Kouba, K. and Tessier, N., "The Dependence of Wall Thickness on Changes in Material and Process Conditions in Plug Assist Thermoforming", SPE's ANTEC Conference Proceedings, 817 – 821 (2009)

Haugstad, G., Gladfelter, W., Weberg, E., Weberg, R. and Jones, R., "Probing Molecular Relaxation on Polymer Surfaces with Friction Force Microscopy", Langmuir, 11, 3473 – 3482 (1995), DOI:10.1021/la00009a033

Hegemann, B., Eyerer, P., "Various Plug Assist Materials and their Effect on the Thermoforming Characteristics of Polymeric Sheet", SPE's ANTEC Conference Proceedings, 707 – 711 (2002)

Hegemann, B., Eyerer, P., "Polymer "Polymeric Friction At Temperatures and Rates Simulating the thermoforming Process", SPE's ANTEC Conference Proceedings, 791 – 796 (2003)

Heuberger, M., Luengo, G. and Israelachvili, J., "Tribology of Shearing Polymer Surfaces. 1. Mica Sliding on Polymer (PnBMA)", J. Phys. Chem. B, **103**, 10127 – 10135 (1999), DOI:10.1021/jp991098a

Hosseini, H., Azemati, A. A, "Rheological Modeling for Production of High Quality Polymeric", World Academy of Science, Engineering and Technology, **47**, 645 – 549 (2010)

Jalham, I. S., "Process Control and Quality Improvement of Plug-Assist Thermoforming Process: A Case Study", Journal of King Abdulazziz University: Eng. Sci., **16**, 17 – 33 (2005)

Karamanou, M., Warby, M., and Whiteman, J., "Computational Modelling of Thermoforming Processes in the Case of Finite Viscoelastic Materials", Comput. Methods Appl. Mech. Eng., **195**, 5220 – 5238 (2006), DOI:10.1016/j.cma.2005.10.029

Kittikanjanaruk, T., Patcharaphun, S., "Computer Simulation and Experimental Investigations of Wall-Thickness Distribution in High Impact Polystyrene and Amorphous Polyethylene Terephthalate Thermoformed Parts", Kasetsart J. (Nat. Sci.), **47**, 302 – 309 (2013)

Lappin, J. F., Harkin-Jones, E. and Martin, P., "Finite Element Modeling of the Plug-Assisted thermoforming Process", SPE's ANTEC Conference Proceedings, 826 – 830 (1999)

Lee, J. K., Virkler T. and Scott, C., "Effects of Rheological Properties and Processing Parameters on ABS Thermoforming", Polym. Eng. Sci., **41**, 240 – 261 (2001), DOI:10.1002/pen.10725

Luengo, G., Heuberger, M. and Israelachvili, J., "Tribology of Shearing Polymer Surfaces. 2. Polymer (PnBMA) Sliding on Mica", J. Phys. Chem. B, **104**, 7944 – 7950 (2000), DOI:10.1021/jp0005773

Maeda, N., Chen, N., Tirrel, M. and Israelachvili, J., "Adhesion and Friction Mechanisms of Polymer-On-Polymer Surfaces", Science, **297**, 379 – 382 (2002), DOI:10.1126/science.1072378

Marchal, T. M., Clemeur, N. and Agarwal, A. "Optimization of the Thermoforming Process: A Few Industrial Examples", SPE's ANTEC Conference Proceedings, 701 – 705 (1998)

Martin, P. J, Duncan, P., "The Role of Plug Design in Determining Wall Thickness Distribution in Thermoforming", Polym. Sci. Eng., **47**, 804 – 813 (2007), DOI:10.1002/pen.20757

Martin, P. J., McCool, R., Harter, C. and Choo, L., "Measurement of Polymer-To-Polymer Contact Friction in Thermoforming", Polym. Sci. Eng., **52**, 489 – 498 (2012), DOI:10.1002/pen.22108

Martin, P. J., Choo, H., Cheong, C. and Harkin-Jones, E., "Plug Materials for Thermoforming: The Effects of Nonisothermal Plug Contact", SPE's ANTEC Conference Proceedings, 812 – 816 (2009)

McCool, R., Martin, P. and Harkin-Jones, E., "Process Modelling for Control of Product Wall Thickness in Thermoforming", Plast. Rubber Compos., **35**, 340 – 347 (2006), DOI:10.1179/174328906X143859

McCool, R., Martin, P., "The Role of Process Parameters in Determining Wall Thickness Distribution in Plug-Assisted Thermoforming", Polym. Sci. Eng., **50**, 1923 – 1934 (2010), DOI:10.1002/pen.21718

McCool, R., Martin, P., "Thermoforming Process Simulation for the Manufacture of Deep-Draw Plastic Food Packaging", J. Process Mechanical Engineering, 225, 269 – 279 (2011), DOI:10.1177/0954408911416292

Michel, D., Marsaudon, S. and Aime, J., "Tribology of a Polystyrene Polymer Film Investigated with an AFM", Tribol. Lett., **4**, 75 – 80 (1998), DOI:10.1023/A:1019130516466

Mieghem, B. V., Lava, P., Debruyne, D., Bael, A. and Ivens, J., "Digital Image Correlation for On-Line Wall Thickness Measurements in Thick Gauge Thermoforming", Key Eng. Mater., **554** , 1583 – 1591 (2013), DOI:10.4028/www.scientific.net/KEM.554-557.1583

Morales, R. A., Candal, M., Santana, O., Gordillo, A. and Salzar, R., "Effect of the Thermoforming Process Variables on the Sheet Friction Coefficient", Mater. Des., **53**, 1097 – 1103 (2014), DOI:10.1016/j.matdes.2013.08.009

Morales, R. A., Candal, M. V., "Plug Material and Sheet Temperature Effect over the Force Penetration Curves under Biaxial Deformation", SPE's ANTEC Conference Proceedings, 2194 – 2199 (2009)

Nam, G. J., Lee, J. and Ahn, K., "Three-Dimensional Simulation of Thermoforming Process and Its Comparison with Experiments", Polym. Eng. Sci., **40**, 2232 – 2240, (2000), DOI:10.1002/pen.11355

Nied, H. F., Taylor, C. and Delorenzi, H., "Three-Dimensional Finite Element Simulation of thermoforming", Polym. Sci. Eng., **30**, 1314 – 1322 (1990), DOI:10.1002/pen.760302009

O'Connora, C. P. J., Martin, P., Sweeney, J., Menary, G., Caton-Rose, P. and Spencer, P., "Simulation of the Plug-Assisted Thermoforming of Polypropylene Using a Large Strain Thermally Coupled Constitutive Model", J. Mater. Process. Technol., **213**, 1588 – 1600 (2013), DOI:10.1016/j.jmatprotec.2013.02.001

Poller, S., Micheali, W., "Film Temperature Determine the Wall Thickness of Thermoformed Parts", SPE ANTEC Tech. Papers, **38**, 104 – 108 (1992)

Schaeffler, D. J., Vineberg, E. J., "Troubleshooting Formability Problems Using Strain Analysis", ASM Handbook, Metalworking: Sheet Forming, Chapter 66, ASM International, **14B**, 697 – 706 (2006:2009)

Sills, S., Tomko, G. and Overney, R. "Molecular Dissipation Phenomena of Nanoscopic Friction in the Heterogeneous Relaxation Regime of a Glass Former", J. Chem. Phys., **123**, 134902-1 – 134902-6 (2005)

Sowerby, R., Chu, E. and Duncan, J. "Determination of Large Strains in Metal Forming", J. Strain Anal. Eng. Des., **17**, 95 – 101 (1982), DOI:10.1243/03093247V172095

Tessier, N., "Thermoformed Trays: How Plug Assists Play a Crucial Role in Package Design, Material Distribution and Product Safety", Therforming Quarterly, **33**, 8 – 10 (2014)

Throne J. L.: Technology of Thermoforming, 1st Edition, Hanser Gardner, Cincinnati, Munich (1996), DOI:10.3139/9783446402478

Throne, J. L., "Modeling Plug-Assist Thermoforming", Adv. Polym. Tech., **9**, 309 – 320 (1989), DOI:10.1002/adv.1989.060090405

Throne, J. L., "Plug-Assist Thermoforming – A New Design Protocol for Rectangular Parts", Polym. Plast. Tech. Eng., **30**, 701 – 721 (1991), DOI:10.1080/03602559108020145

Tulsian, A., Mead, J., Orroth, S. and Tessier, N., "Computer Simulation of the Effect of Coefficient of Friction in Plug Assist Thermoforming", SPE's ANTEC Conference Proceedings, 904 – 908 (2004)

Warby, M. K., Whiteman, J. R., Jiang, W. G., Warwick, P. and Wright, T., "Finite Element Simulation of Thermoforming Processes for Polymer Sheets", Math. Comput. Simul., **61**, 209–218 (2003), DOI:10.1016/S0378-4754(02)00077-0

Warby, M. K., Whiteman, J. R., "Finite Element Model of Viscoelastic Membrane Deformation", Comput. Methods Appl. Mech. Eng., **68**, 33–54 (1988), DOI:10.1016/0045-7825(88)90105-3

Weische, S., "Industrial Thermoforming Simulation of Automotive Fuel Tanks", Appl. Therm. Eng., **24**, 2391–2409 (2004), DOI:10.1016/j.applthermaleng.2004.03.003

Yoshizawa, H., Chen, Y. and Israelachvili, J., "Fundamental Mechanisms of Interfacial Friction. 1. Relation between Adhesion and Friction", J. Phys. Chem., **97**, 4128–4140 (1993), DOI:10.1021/j100118a033

Acknowledgements

This research was generously funded by the Department of Chemicals and Petrochemicals (DCPC) of the Ministry of Chemicals and Fertilizers, Govt. of India and was sponsored through the Center of Excellence-Sustainable Polymer Industry for Research Innovation and Training (CoE-SPIRIT). Also, the authors would like to thank Dr. Pramod Joshi, Polymer Engineering Department, MIT, Pune for making available the thermoforming machine for this research and also his valuable inputs. Also, the authors will like to thank Compuplast Inc., Canada for providing academic license to T-SIM.

Date received: December 28, 2014
Date accepted: October 23, 2015

Bibliography
DOI 10.3139/217.3060
Intern. Polymer Processing
XXXI (2016) 2; page 166–178

ISSN 0930-777X